

Discovering hidden layers in quantum graphs

Lukasz G. Gajewski* and Julian Sienkiewicz

Faculty of Physics, Warsaw University of Technology, Koszykowa 75, 00-662 Warszawa, Poland

Janusz A. Hołyst

*Faculty of Physics, Warsaw University of Technology, Koszykowa 75, 00-662 Warszawa, Poland and
ITMO University, Kronverkskiy Prospekt 49, St Petersburg, Russia 197101*

Finding hidden layers in complex networks is an important and a non-trivial problem in modern science. We explore the framework of quantum graphs to determine whether concealed parts of a multi-layer system exist and if so then what is their extent, i.e. how many unknown layers there are. We assume that all information we have is the time evolution of a wave propagation on a single layer of a network and show that it is indeed possible to uncover that which is hidden by merely observing the dynamics. We present evidence on both synthetic and real world networks that the frequency spectrum of the wave dynamics can express distinct features in the form of additional frequency peaks. These peaks exhibit dependence on the number of layers taking part in the propagation and thus allowing for the extraction of said number. In fact, with sufficient observation time, one can fully reconstruct the row-normalized adjacency matrix spectrum. We compare this approach to the work of Aziz et al. in which there has been established a wave packet signature method for discerning between various single layer graphs and we modify it for the purposes of multi-layer systems.

I. INTRODUCTION

A plethora of contemporary dynamical systems and collective phenomena can be expressed in terms of complex networks and recently often with multi-layer models. Whether it is a transportation network (e.g. buses and trams) or a social one (e.g. Twitter and Facebook) various forms of information propagation or state dynamics can be described with multi-layer networks. [1–7]

However, it is not uncommon for certain parts of a system to remain hidden from observers and it can be crucial to be able to discern what characteristics are unknown and then to try to obtain them. Such inverse problems have been studied in various settings in both topology and dynamics parameters reconstruction in mono- and multi-layer scenarios alike [8–20]. Recently there has been some pivotal advances in terms of determining whether one can detect hidden layers in non-markovian dynamics and even obtain how many of these layers are there [21].

Nevertheless, to our knowledge, there has not been much done specifically for uncovering the multi-layer structures in quantum graphs and thus we address this issue and present two potentially viable approaches of establishing if hidden layers exist and in some scenarios to ascertain the exact count of these layers.

Traditionally graphs are discrete, combinatorial abstract mathematical objects. If we supply them with a metric and topology we call such objects *metric graphs*. Those in turn equipped with a second order differential operator acting on its vertices and edges - a Hamiltonian - and appropriate boundary conditions are called

quantum graphs [22–25]. It is worth underlining here that with this definition we do not specify the exact nature of the Hamiltonian and while it is often a quantum mechanical one it need not be so and thus here we follow the interpretation of taut strings, fused together at the vertices that can be seen as the “limiting case” of a “quantum wire” [26, 27]. The (most likely) first use of this framework can be traced back to Pauling’s paper in 1936 [28], however, for the most part quantum graphs have not been widely used until more recently. Nowadays they see many various applications in dynamical systems, nanotechnology, photonic crystals and many others [29–34]. Most recently Aziz et al. established a method based on a wave packet propagation on quantum graphs that allows to distinguish between structures in complex networks [35] thanks to many well studied properties of the Laplacian (e.g. finite speed of propagation [36] as opposed to a discrete Laplacian [37, 38]) and its spectra in quantum graphs [39–45]. The idea of determining the shape of an object based on observable dynamics on it goes back to the work of Kac in 1966 [46] in which he asks whether it is possible to hear the shape of a drum. Giraud and Thas showed that the eigenvalues of different shapes can be identical and therefore answered Kac’s question in the negative. Gutkin and Smilansky, on the other hand, showed that in quantum graphs specifically, under certain conditions, one can indeed “hear” the shape as the Hamiltonian uniquely defines the connections and their lengths when the graph is finite (and simple), the bond lengths are rationally independent and the vertex scattering matrices are properly connecting. It is also worth noting that this inverse spectral problem can be extended onto scattering systems as also stated in the same paper (a so called inverse scattering problem [47]), however, in this case it is *not* always possible [48, 49] (i.e. there is a way to construct isoscattering pairs of graphs

* lukaszgajewski@tuta.io

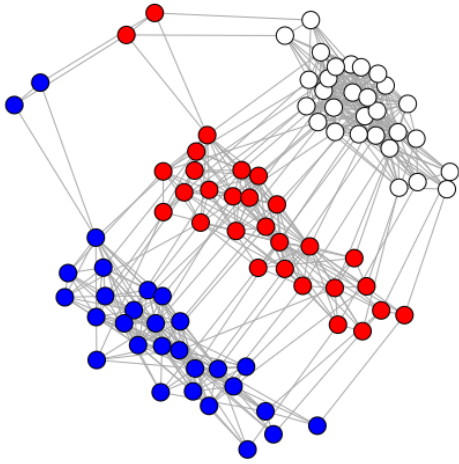


FIG. 1. Three-layered multiplex representation of the Vickers [54] data.

with identical polar structure of their scattering matrices) which was also showed experimentally via microwave networks by Hul et al. [50]. Wave packets specifically has also attracted some attention in recent years but not for the purposes of the goal we aim for in this paper [51, 52]. Some work has been done in context of sufficient coverage with sensors [53], however, in this case we also will not share all the assumptions and thus those methods are not applicable to our problem.

In this paper we tackle the problem of determining whether there are hidden layers in the complex system we are observing and if so then how many. We assume a wave packet propagation dynamics on a quantum graph as our model for the dynamical system. Each edge e in the graph G has an associated length $l_e = 1$ and a spatial coordinate variable $x_e \in [0, l_e]$ along said edge. We use a special case of a Hamiltonian - an edge based Laplacian giving us an edge-based wave equation on a graph in the form:

$$u_{tt}d\mathcal{E} = -\Delta u \quad (1)$$

where \mathcal{E} is a Lebesgue measure on the graph's edges [26, 55].

We use Neumann boundary conditions stating that the sum of outward pointing gradients at every vertex must vanish [26, 35]:

$$\forall v \in G, \sum_{e \ni v} (-1)^{1-x_{e,v}} \nabla f(e, x_{e,v}) = 0 \quad (2)$$

The initial condition for the wave equation is Gaussian wave packet:

$$f(e, x) = \exp(-a(x - \mu)^2) \quad (3)$$

which is fully contained within a single edge with the highest betweenness centrality[56] following the conventions of Aziz et al [35]. We simulate many layer system in

a multiplex configuration, i.e. each node is connected to its reflection in a neighbouring layer (see Fig. 1 for a real world network example and Fig 2 for wave propagation example on a simple synthetic graph). While the propagation simulations are computed on full systems, for the detection purposes we always only use information from a single layer, i.e. all but one layer are hidden from the perspective of our methods at all times.

This rest of the paper consists of three main parts followed by a discussion. Firstly we briefly outline the approach introduced by Aziz et al. in [35] and show its viability for the purposes of multi-layer networks in the context described above. Secondly we introduce our own approach with the use of a Fourier transform on the time evolution of sum of amplitudes in the visible part of the system. Thirdly, we show that with sufficient resources (i.e. observation time) one can fully reconstruct the spectrum of the row-normalized adjacency matrix.

II. GAUSSIAN WAVE PACKET SIGNATURE (WPS)

Gaussian wave packet signature (WPS) is a methodology developed by Aziz et al. [35] that allows to distinguish between various types of graphs. The procedure starts by initiating an edge with a Gaussian wave packet that is completely contained on said edge (see Fig. 2a). The edge is chosen to be one with highest betweenness centrality as to assure fastest possible spread of the wave on the graph (although this can, of course, be relaxed in general). Then on each integer time we measure the amplitude in the centre of every edge $2|E|$ times in total, where $|E|$ is the number of edges (see Fig. 2b and Appendix A for a detailed description of the way the amplitude is calculated). We measure the centre of each edge because at integer times the highest value is in the centre. Finally create a histogram with 100 bins of these measurements - this is the WPS of the graph. Aziz et al. show that particular graph types (say Barabási-Albert, Erdős-Rényi etc.) will have similar WPSs yet different in comparison to other types (so e.g. one can differentiate an ER from BA). In order to actually do this differentiation one must build a classifier. In their work a K-nearest neighbours (K-NN) classifier was chosen. From the perspective of the machine learning tools we use in this paper (K-NN, PCA) each histogram bin of the WPS is a dimension in the feature space.

For our purposes we will deviate slightly from this procedure. Namely to us the whole graph is not known and the graph itself is a multiplex. Additionally we assume that the wave propagation is an actual process ongoing through some the network. Thus, we assume we have access to a single layer on which a certain spread has happened that can be modelled with a Gaussian wave packet and we suspect there may be hidden layers in the network. Question is - can we detect their presence?

The rest of the procedure is similar, i.e. we create a

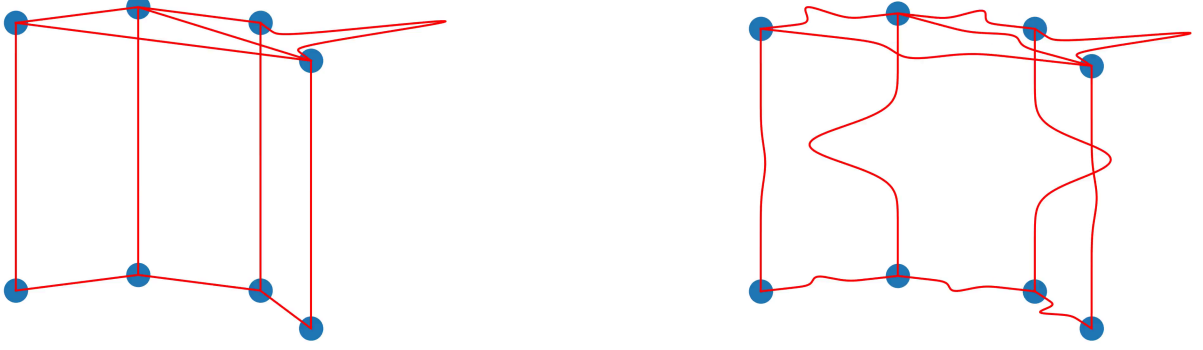


FIG. 2. An exemplary picture of a wave starting at a specific edge (left, $t = 0$) and then propagating through the multiplex system (right, $t > 0$).

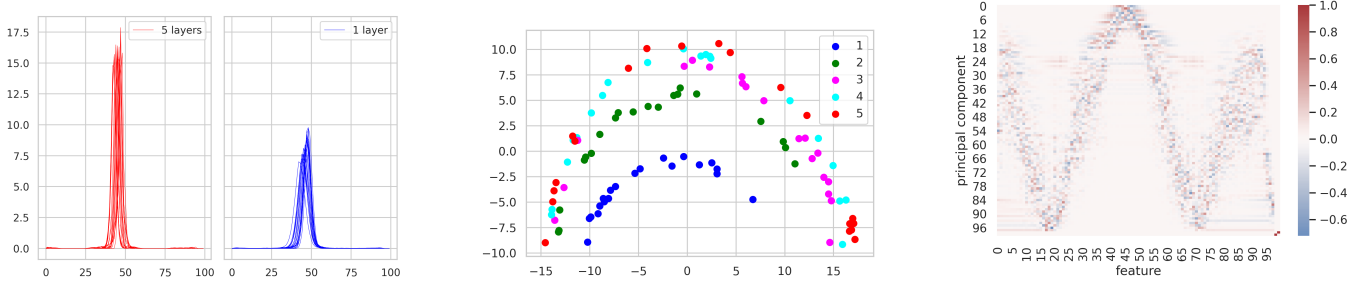


FIG. 3. Wave packet signatures (left) for various realisations of a Barabási-Albert ($N = 50$, $m = 3$) graph with 5 and 1 layers (measured on one layer only). WPS projected onto a 2D space with PCA (centre) with colours distinguishing no. of layers. Each point is a different BA graph. PCA transformation matrix (right) showing the contributions of given WPS bins into principal components.

WPS and we train a classifier on a given type of a graph (e.g. BA) and this time the classes are the number of layers. See Fig. 3 and 4 where we compare WPSs of a 5-layer BA graph vs 1-layer and a 5-layer ER graph vs 1-layer respectively. One can clearly see that the signatures are distinct. To further illustrate this we use Principal Component Analysis (PCA, see Appendix B for details) to project the WPSs onto a 2D space (see the centre pieces of Fig. 3, 4). There one can see that each class takes a distinct region of space and thus we should be able to discriminate between them. However, it is worth noting that the more layers there are the more tightly packed the observations are, i.e. discriminating between mono-layer and penta-layer graphs is fairly easy, between tetra- and penta- not as much. It is also worth noting that through PCA we can see that the centre bins carry the most variance in the feature space (see panels on the right in Fig. 3, 4) and that there are certain distinct structures visible in the higher PCs for both BA and ER graphs.

As mentioned before, we follow Aziz et al. and also choose the K-NN for classification (see Appendix C for a description of the K-NN method). We build the model

on various graphs with between 1 to 5 layers (with values only from one layer each time as explained earlier) and then test it to see if it can recognise how many layers there are in an unknown graph. We conducted our tests for BA and ER graphs (see Fig. 5 for results of classification). For each type of graph we simulated 500 independent realisations (100 per each number of layers) with mean degree $\langle k \rangle = 6$ and network size $N = 50$. We take out a 100 randomly chosen, in a stratified manner (i.e. classes are equally represented), realisations are taken out of the training set (this will be the test set). On the training set we conduct 100 rounds of training and then testing. That is in each round we do the training/test split, then a 10-fold cross-validation on the training set to find the best K parameter of the K-NN model and then use that on the test set. We present the results in a form of box plots. In Fig. 5 we show the accuracy of the classifier for both BA and ER. We can see that while for ER the results are slightly lower than for BA, in both cases the accuracy is still fairly high with medians of 92 and 89 for BA and ER respectively.

To additionally illustrate the point made earlier that higher numbers of layers are more difficult to discern

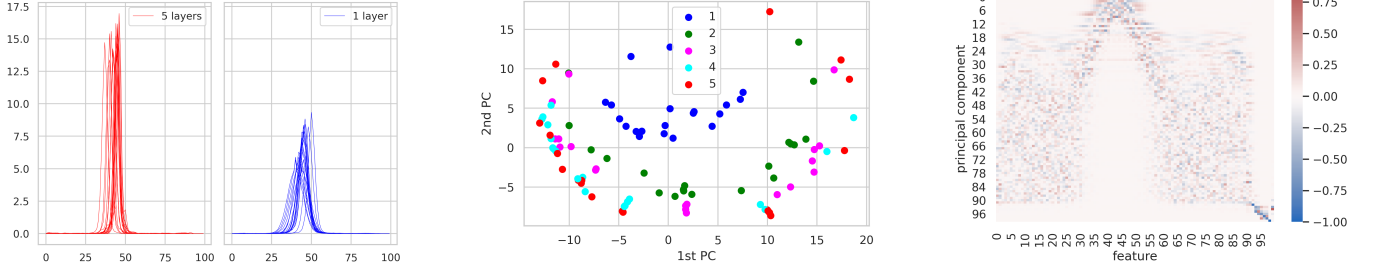


FIG. 4. Wave packet signatures (left) for various realisations of a Erdős-Rényi ($N = 50$, $\langle k \rangle = 6$) graph with 5 and 1 layers (measured on one layer only). WPS projected onto a 2D space with PCA (centre) with colours distinguishing no. of layers. Each point is a different ER graph. PCA transformation matrix (right) showing the contributions of given WPS bins into principal components.

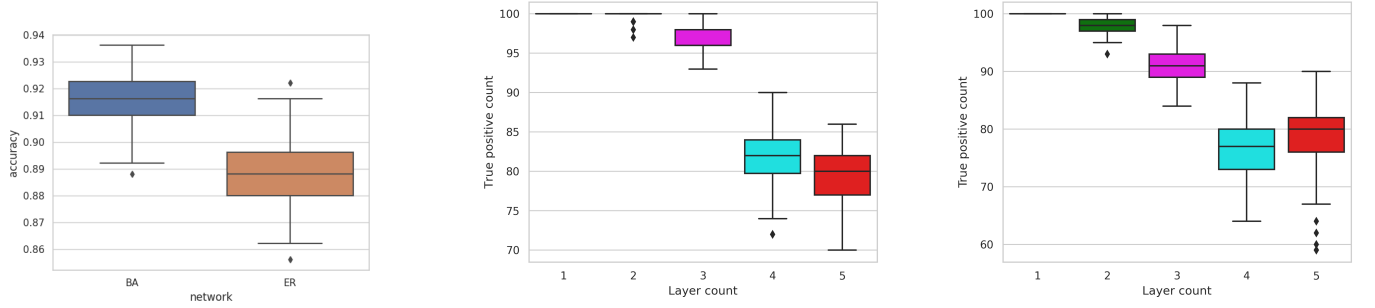


FIG. 5. K-nearest neighbours classification accuracy of the layer count for a BA and ER graph as box plots (left) based on single layer WPSs. Contingency table diagonal values as box plots for a BA (centre) and ER (right). We simulated 400 independent realisations of a given graph type (BA, $N = 50$, $m = 3$; ER, $N = 50$, $\langle k \rangle = 6$). For each type of graph we conducted 100 rounds of 10-fold cross-validation to determine the K parameter in K-NN withdrawing 100 realisations (25%) for purposes of final evaluation. Train/test split was random and stratified.

amongst one another we show the diagonal values of contingency tables from all 100 rounds for BA (centre panel of Fig. 5) and ER (the right panel of Fig. 5). One can clearly see that identifying mono-layer systems is practically 100% accurate and it is the more layered systems that cause trouble for the classifier.

While the classification results seem very promising it is important to note the obvious and major disadvantage of this approach. One must build a training set for it to work. With synthetic networks it is easy to generate as many as one wants and the limitation is purely computing power. When dealing with real world networks one often does not simply have the ability to have similar enough graphs to the one currently under observation but with added layers. In such a circumstance perhaps a combination of many different synthetic networks could suffice and other, more advanced, classification methods than K-NN could be utilised. That, however, is beyond the scope of this study.

III. FOURIER TRANSFORM OF THE AMPLITUDE SIGNAL

Here we introduce a new approach to detecting layers on quantum graphs. Similarly to the previous case we assume we can either produce or observe a wave propagation on the graph initiated by a Gaussian wave packet. For efficiency's sake in the simulations used we used the edge with highest betweenness centrality as before and we also measure the amplitudes at integer times in the centres of all edges for $2|E|$ times. While in WPS method we simply follow the advice of Aziz et al. for the count of measurements in the approach discussed here it is usually rather clear if enough data was collected by straight forward visual inspection.

Our proposition is as follows, at each integer time compute the sum of all amplitudes in the visible part of the system and treat it as a time dependent signal $S(t)$. Transform the signal into frequency domain via a fast Fourier transform (see Appendix D and [57]) - $\hat{S}(f)$ - and look at the spectrum of the signal - $|\hat{S}(f)|^2$.

A mono-layer system will produce a “flat” signal $S(t)$ whilst multi-layer one will exhibit periodic behaviours due to energy leaking in and out of the visible layer from and into other layers. At sufficiently long measurement

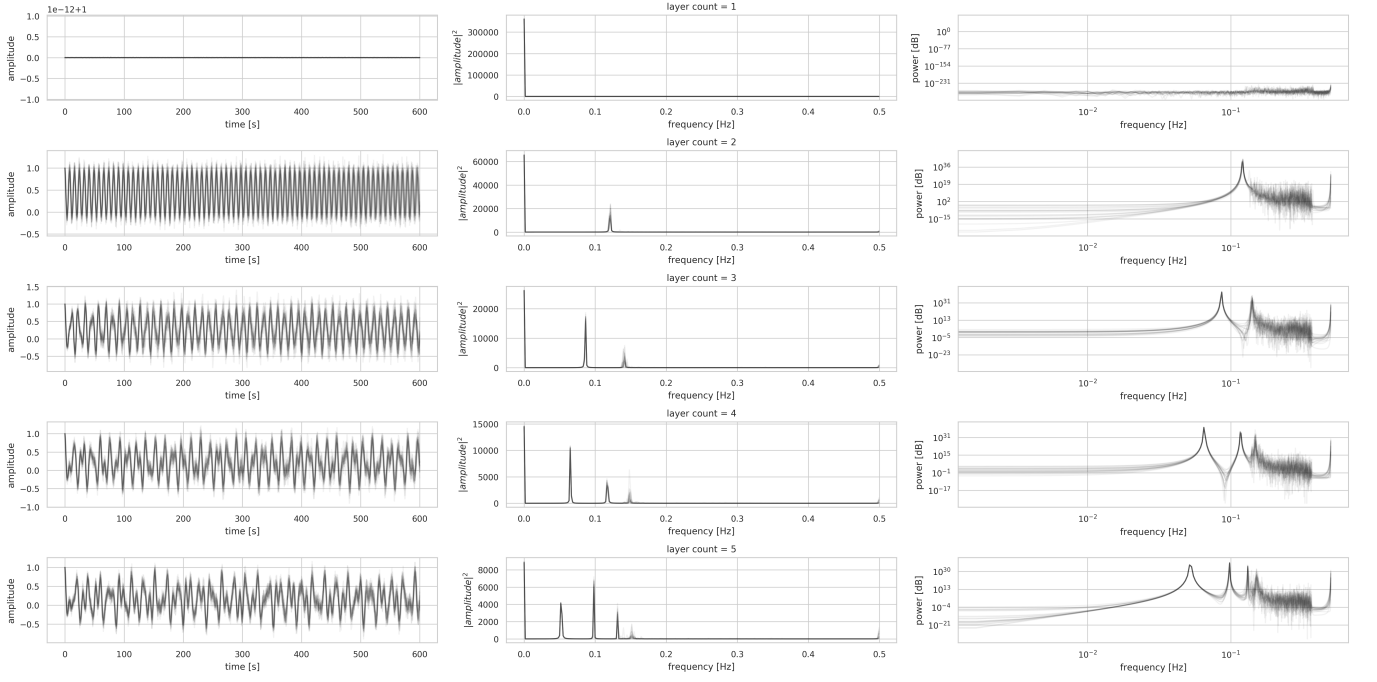


FIG. 6. Sum of amplitudes time evolution as measured on the only visible layer (left). Fast Fourier transform of this signal (centre) and its power spectrum (right). Each row represents a different number of layers (1 to 5 going top to bottom). Simulations conducted on 20 independent realisations of a BA graph ($N = 50$, $m = 3$) per row, overlaid with transparency.

time scale the signal should stabilise and become stationary as long as no perturbation is introduced to the overall network. This transfer of energy induces oscillations in the amplitude sum on the visible layer which in turn create clear peaks in the power spectrum, see Fig. 6 for results from BA graphs and 7 for ER. Left column shows the signal $S(t)$, centre $|\hat{S}(f)|^2$ and right $|\hat{S}(f)|^2$ in decibels and log-log scale. Each row has 20 independent realisations plotted on top of each other with transparency to show that these peaks are fairly consistent, and different number of layers (1st row are mono-layer systems, 2nd row di-layer etc.). It is quite apparent that there are visible peaks and their count strictly corresponds to the number of layers in the system.

These results already show the advantage of FFT over WPS as it is simpler and does not seem to suffer from struggling to differentiate as much between high-layer systems. Additionally it does not require any prior knowledge or learning of the model. It is far from flawless, however. As it is much easier to test on real networks than WPS we applied it to three real world networks [54, 58, 59] - see descriptions in Appendix E. The results are in Fig. 9 where one can see that while we do get peaks in the spectrum and therefore can confidently state that there are hidden layers, it is much less clear how many of them there are. This is most likely due to the fact that these networks are not as clear cut multiplexes as the synthetic systems we discussed earlier. These networks here have various mean degrees in each layer and that also implies varied coupling strength between the layers.

Additionally real world networks can have other characteristics different between the layers such as clustering coefficients or degree distributions and the synthetic systems tested simply do not have this property. However, we show in the next section that it is possible to reconstruct the full spectrum of the row-normalized adjacency matrix with this method and therefore determine the number of layers for any system.

IV. SPECTRUM RECONSTRUCTION

In this section we show that with sufficiently long observation it is possible to completely recover all eigenvalues of row-normalized adjacency matrix of the full system and thus trivially determine the number of hidden layers.

We shift slightly from previous sections as we no longer take measurements on the edges but only on nodes. This makes the problem less computationally intensive and also, in our opinion, makes for a more practical case as it might be sometimes easier to observe just the nodes' states. However, same analysis can be applied using edge measurements as previous sections could be done with node values only - we chose otherwise as we are stemming from the work of Aziz et al.

Similarly as before we observe the sum of amplitudes, however, in this case it is important to have enough samples of the signal to provide sufficient resolution in the power spectrum. How long one needs to observe a system will of course depend on the intricacies (and mostly

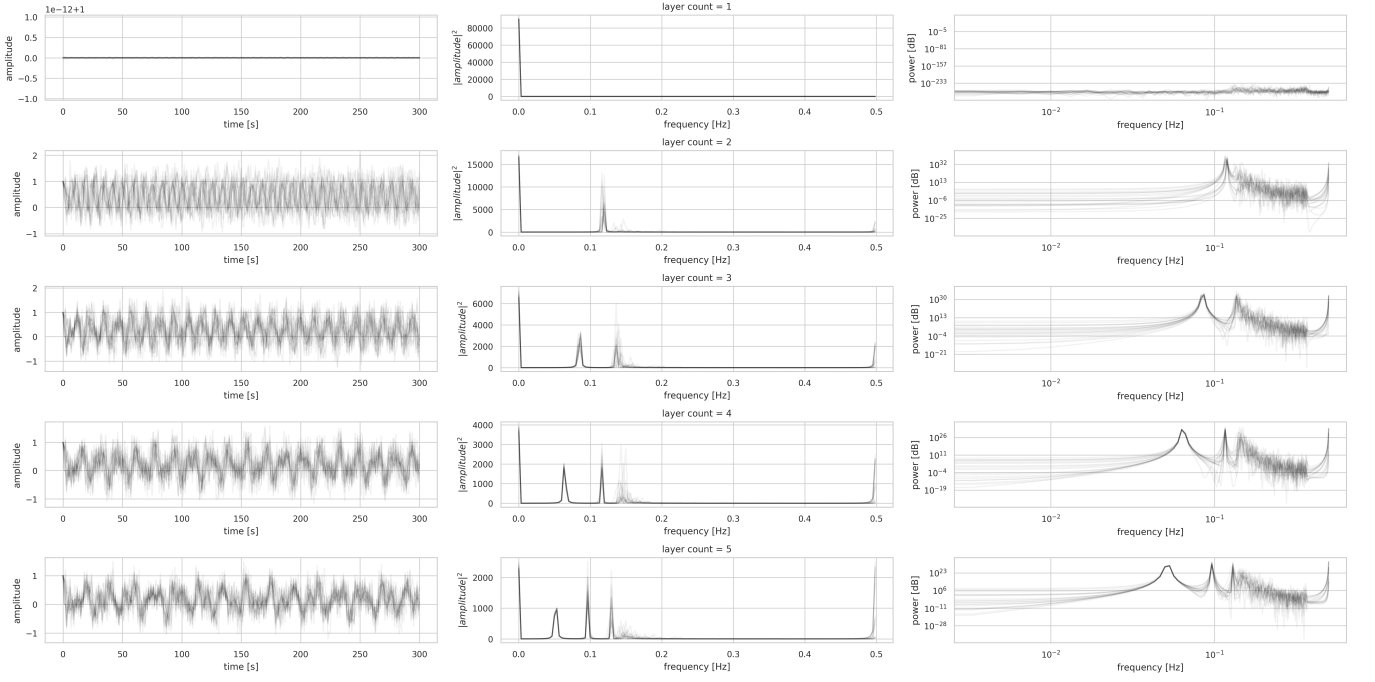


FIG. 7. Sum of amplitudes time evolution as measured on the only visible layer (left). Fast Fourier transform of this signal (centre) and its power spectrum (right). Each row represents a different number of layers (1 to 5 going top to bottom). Simulations conducted on 20 independent realisations of an ER graph ($N = 50$, $\langle k \rangle = 6$) per row, overlaid with transparency.

size) of the system in question. As the propagation process is not stochastic the time needed for observation is finite and in our experience not unattainable. The goal is simply to have the complete power spectrum of the signal. Then one takes note of the peaks present - we opted for an automated approach using a wavelet transform [60] (see Appendix F). It turns out that the peaks in the power spectrum are the eigenvalues of the Hamiltonian (divided by 2π) which in turn are directly related to the eigenvalues of the row-normalized adjacency matrix - \hat{A} - such that each eigenvalue $\lambda \notin \{-1, 1\}$ of \hat{A} has corresponding Hamiltonian eigenvalues $\cos^{-1}(\lambda)$ and $2\pi - \cos^{-1}(\lambda)$. This leads us to two important results, i) the number of frequencies present in the power spectrum $\#f$ is two less than count of eigenvalues of the adjacency matrix and since we know the layer sizes (i.e. node count per layer - N) as a multiplex structure was assumed the number of layers $K = (\#f + 2)/N$. ii) we can in fact recover almost exactly all eigenvalues of \hat{A} as $\cos(2\pi f_i)$ for each frequency peak f_i in the power spectrum.

We present the result of the full spectrum reconstruction on Fig. 8 for a complete, BA and real world graph. We chose the complete graph as it has a special case due to the extreme symmetries of the multiplex adjacency matrix and thus the number of peaks directly corresponds to the number of layers unlike more complex cases where the eigenvalues multiplicities behave differently. Of course, this does imply that if due to specific structures in a given system some eigenvalues have high multiplicity the simple formula $K = (\#f + 2)/N$ will not hold

and system specific adjustments would be needed. The reconstructed eigenvalues give an almost perfect match with those of the row-normalized adjacency matrix. Note that the performance here is mostly limited by the peak detection method and the resolution in the frequency domain, i.e. the information is there in the spectrum, the only challenge is to recover it efficiently.

V. DISCUSSION

In this paper we explore the paradigm of quantum graphs as a potential tool for studying multi-layer networks. The particular problem we are interested in is determining whether there are hidden layers of communication in the system that we cannot observe by taking measurements of the ongoing dynamics in the single layer that we can observe. We proposed and tested two methods - one based upon a Gaussian wave packet signature (WPS) that was introduced prior by Aziz et al. to discriminate between various types of mono-layer systems and the other on observing the power spectrum of the wave amplitudes.

WPS is a method where a Gaussian wave packet, either observed or purposefully produced, initiates the propagation from a single edge and we take measurements of amplitudes at every edge at integer times sufficiently long. Such data is then histogrammed to produce the signature. This signature has the property of being similar within a category of graphs (originally e.g. ER vs BA,

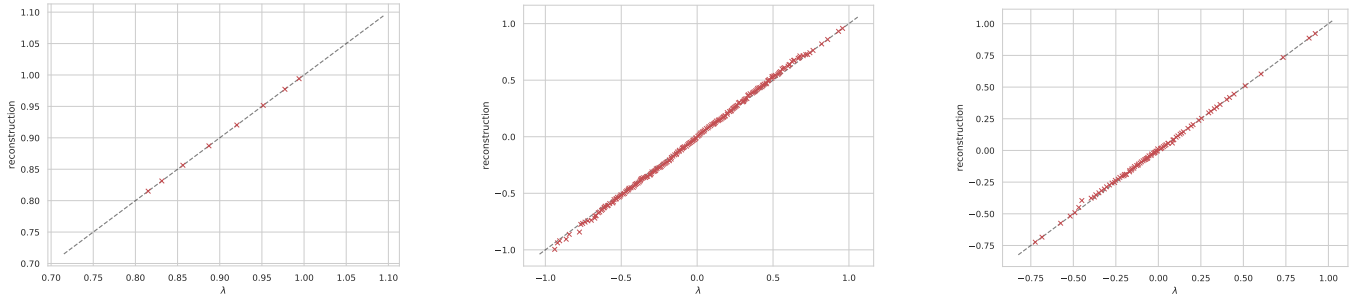


FIG. 8. Eigenvalues reconstruction from the Fourier spectrum of the nodes' amplitudes sum signal. (Left) an example of a complete graph multiplex with layer size $N = 20$ and number of layers $K = 9$. As it is a special case of an extremely symmetric adjacency matrix there are only as many eigenvalues as there are layers. (Right) a Barabási-Albert graph with $N = 50$, $m = 3$, $K = 4$ has a much more complex spectrum and so does a real world network (right) - Vickers[54] - both of which we attain an almost perfect match between the recovered and actual eigenvalues. The dashed diagonal line is a visual aid showing “ $y = x$ ”.

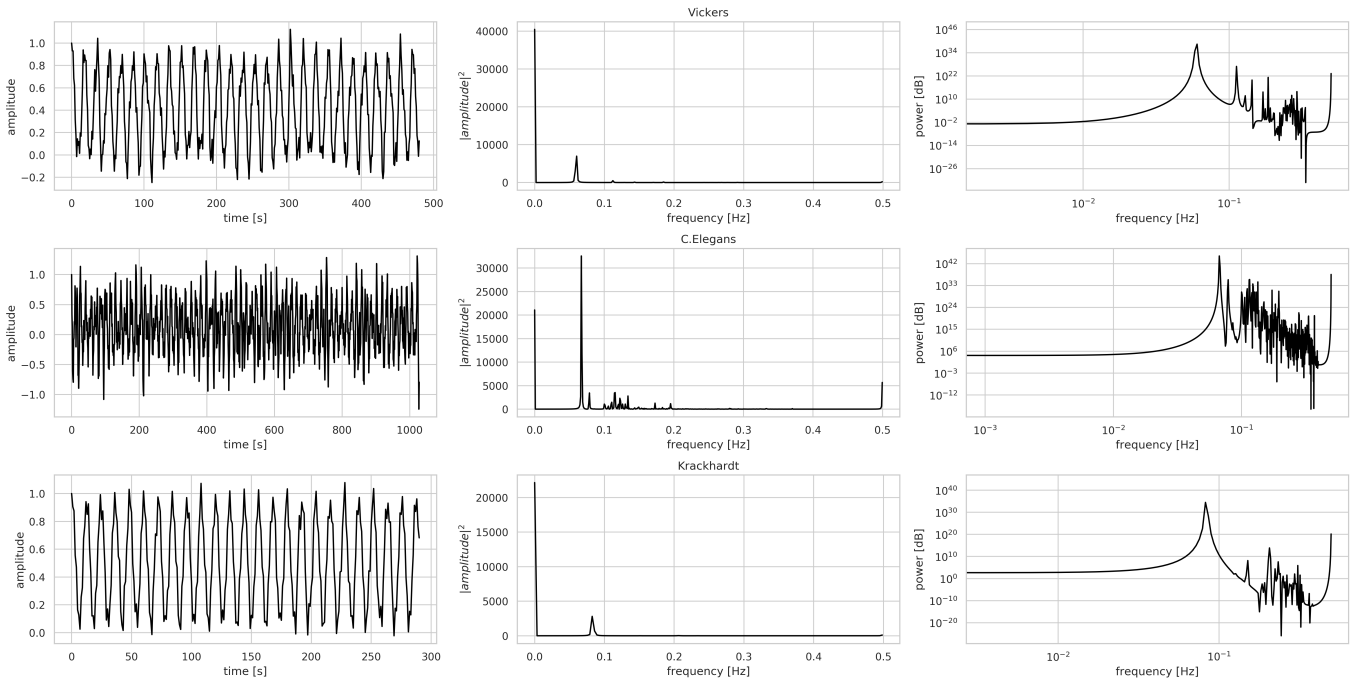


FIG. 9. Sum of amplitudes time evolution as measured on the only visible layer (left). Fast Fourier transform of this signal (centre) and its power spectrum (right). Each row represents a different real world network (as indicated by titles - Vickers[54], C.Elegans[59], Krackhardt[58]). Each graph is a 3-layered multiplex.

here number of layers) while varied without. This in turn can be utilised by machine learning models, such as K-nearest neighbours, to build a model capable of discriminating between graphs with different number of layers. This approach suffers from several issues. Most prominently it requires a training sample. This can be very difficult to obtain in real world scenarios and while perhaps a well varied synthetic data set could suffice at this point it is a mere speculation. The choice of appropriate machine learning scheme and its construction is also a non-trivial task. Additionally as the number of layers grows differentiating between such networks becomes

increasingly difficult since the signatures become less varied.

We also introduce an approach that utilises a discrete Fourier transform (DFT) instead of a machine learning model. Instead of histogramming the measurements as before one computes the sum of amplitudes on the visible layer at each integer time. This constitutes a signal that at sufficient time scales should become stationary. In a mono-layer system the signal will simply be a constant value due to energy conservation. However, should other layers be in the system from the perspective of the mono-layer there will be oscillations as the

energy will flow out and back into it. We can inspect those oscillations with the use of DFT and look at the power spectrum. The spectrum will exhibit characteristic peaks absent in mono-layer networks. The number of these peaks strictly corresponds with the number of layers in the synthetic scenarios tested. This approach is significantly advantageous over the WPS as it does not require building a learning sample and is in general much simpler. Furthermore it does not really suffer in terms of differentiating e.g. tetra- from penta-layer systems etc. Although it shows much promise in synthetic scenarios, it does not perform as well in real world networks. It does indeed indicate clearly that there are hidden layers but the number of them can be rather tricky to discern. This is perhaps not that surprising considering that real world networks are much more “messy” in some way than synthetic examples. Layers vary in size, degree distribution, clustering coefficients and so on and so forth while say a penta-layer BA graph shares all characteristics between layers even though the exact connections are different. Those and other features of real world systems could also affect the coupling amongst the layers that most certainly will affect the nature of the amplitude signal.

In such cases (i.e. where peak count after a brief observation is not enough) we show that simply a longer observation time is required. As the signal is not stochastic and oscillation periods is finite it does not seem unfeasible to observe enough of the signal to determine its power spectrum with sufficient resolution. Then each peak in the spectrum correspond to the Hamiltonian eigenvalues that in turn are related to the eigenvalues of the row-normalized adjacency matrix via simple formula. With this we showed that it is indeed possible to recover all these eigenvalues and thus trivially determine the number of layers in the system.

It is worth underlining here that a row-normalized adjacency matrix is in fact a so called right stochastic matrix of a given graph and while it goes beyond the scope of this paper, there exist methods of reconstructing the whole matrix from its spectrum [61–65] which we suspect should be quite feasible considering we already assume knowing part of it (one layer and inter-layer structure). That in turn could also open the door to the adjacency

matrix itself. Recovering all the connections exactly may not be possible, however, having a matrix isospectral to the adjacency matrix is also very valuable as having this spectrum allows for determining many important properties of the system [66, 67].

We find that both methods presented in this paper - the WPS and FFT - show enough success in these simple scenarios we tested to merit further study, such as in noisy (or stochastic) systems, for instance. They each have their pros and cons that we hopefully managed to outline clearly as well as the potential room for improvement of their applicability and understanding of waves on quantum graphs alike.

ACKNOWLEDGMENTS

This work has been supported by National Science Centre, Poland Grant No. 2015/19/B/ST6/02612.

Appendix A: Calculation of the wave amplitude

1. Overall description

The general solution of the wave equation on graph G , provided that the initial condition is Gaussian packet fully localised on a given edge f is derived and presented in detail by Aziz *et al.* in [35]. Here, we re-write it in terms of integer times, i.e., $t = 0, 1, 2, \dots$ so that it fits the case examined in the main text. We additionally assume that the graph is unweighted, undirected and non-bipartite. In such a setting, we consider an arbitrary edge $e = \{u, v\}$ that connects two vertices u and v and can be associated with a variable $x_e \in [0, 1]$ that represents coordinate along such an edge. Then the amplitude u of the wave in the middle of edge e can be expressed as

$$u(e, f, t) = u_1(e, f, t) + u_5(e, f, t) + \frac{1}{|E|}, \quad (\text{A1})$$

where $|E|$ is the number of edges in the graph and u_1 and u_5 are defined as follows

$$\begin{aligned} u_1(e, f, t) &= \sum_{\omega \in \Omega} C(e, \omega) C(f, \omega) \cos(B(e, \omega) + \frac{1}{2}\omega) \cos(B(f, \omega) + \omega(\frac{1}{2} + t)) \\ u_5(e, f, t) &= 2 \cos(\pi t) \sum_i C_\pi(e, i) C_\pi(f, i) \end{aligned} \quad (\text{A2})$$

In the above equations ω , $C(e, \omega)$ and $B(e, \omega)$ come from the edge-based eigenvalues and eigenfunctions, which are, respectively ω^2 and $\phi(e, x_e) = \pm C(e, \omega) \cos(B(e, \omega) + \omega x_e)$ of the row-normalized adjacency matrix $\hat{\mathbf{A}}$ of the graph G . Assuming that we know vertex-based eigenvector-eigenvalues pairs $(g(v), \lambda)$

of matrix $\hat{\mathbf{A}}$ we can express $C(e, \omega)$ and $B(e, \omega)$ as

$$\begin{aligned} C(e, \omega)^2 &= \frac{g(v, \omega)^2 + g(u, \omega)^2 - 2g(u, \omega)g(v, \omega) \cos \omega}{\sin^2 \omega} \\ \tan B(e, \omega) &= \frac{g(v, \omega) \cos \omega - g(u, \omega)}{g(v, \omega) \sin \omega}, \end{aligned} \quad (\text{A3})$$

while $\omega = \arccos \lambda$. The sign of $C(e, \omega)$ needs to be chosen in order to match the phase, in practice it can be achieved

by calculating $\text{sgn}[g(v)]|C(e, \omega)|$. It is always true that one of the eigenvalues is equal to 1 (consequently, $\omega = 0$): this value is responsible for the constant term $1/E$ in Eq. (A2) so it is not included in further calculations, i.e., it

does not belong to Ω set in function u_1 . Although $\phi(e, x_e)$ are orthogonal, they still need to be normalised. To fulfil this condition for each $\omega \in \Omega$ we calculate normalisation factor $\rho(\omega)$

$$\rho(\omega) = \sqrt{\sum_e C(e, \omega)^2 \left[\frac{1}{2} + \frac{\sin(2\omega + 2B(e, \omega)) - \sin(2B(e, \omega))}{4\omega} \right]} \quad (\text{A4})$$

where e runs over all edges in graph G . Then, in order to obtain properly normalised value of $C(e, \omega)$ one needs to divide it by $\rho(\omega)$.

For calculations of C_π one first needs to transform the original undirected graph G into a directed one $D(G)$ by simply replacing each edge $e = \{u, v\}$ with two arcs (u, v) and (v, u) . In the next step we create a structure called oriented line graph (*OLG*), constructed by substituting each arc of $D(G)$ by a vertex (such vertices are connected if the head of one arc meets the tail of another arc). Using the adjacency matrix \mathbf{A}_{olg} of the *OLG* we solve the eigenproblem $\mathbf{A}_{olg}\mathbf{g}_{olg} = \lambda_{olg}\mathbf{g}_{olg}$ and then restrict ourselves to $\lambda_{olg} = -1$ and corresponding eigenvectors (there should be exactly $|E| - |V|$ linearly independent solutions) that form C_π .

2. An example

In order to make the above concise description clear, let us follow a very simple example of a graph shown in Fig. 10a. In such case, knowing the adjacency matrix \mathbf{A} where $A_{ij} = 1$ if nodes i and j share a link and $A_{ij} = 0$ otherwise, we can write the row-normalised adjacency

matrix $\hat{A}_{ij} = A_{ij} / \sum_k A_{kj}$ as

$$\hat{\mathbf{A}} = \begin{pmatrix} 0 & \frac{1}{3} & \frac{1}{3} & \frac{1}{3} \\ \frac{1}{2} & 0 & 0 & \frac{1}{2} \\ \frac{1}{3} & \frac{1}{3} & 0 & \frac{1}{3} \\ \frac{1}{2} & 0 & \frac{1}{2} & 0 \end{pmatrix}. \quad (\text{A5})$$

Solving the eigenproblem $\hat{\mathbf{A}}\mathbf{g} = \lambda\mathbf{g}$ one obtains in this case the following eigenvectors

$$\mathbf{g} = \begin{pmatrix} \omega_1 & \omega_2 & \omega_3 & \omega_4 \\ 1 & \sqrt{\frac{2}{13}} & \frac{\sqrt{2}}{2} & 0 & -\frac{1}{2} \\ 2 & -\frac{3}{\sqrt{26}} & 0 & -\frac{\sqrt{2}}{2} & -\frac{1}{2} \\ 3 & \sqrt{\frac{2}{13}} & -\frac{\sqrt{2}}{2} & 0 & -\frac{1}{2} \\ 4 & -\frac{3}{\sqrt{26}} & 0 & \frac{\sqrt{2}}{2} & -\frac{1}{2} \end{pmatrix} \quad (\text{A6})$$

and related eigenvalues $\lambda = (-\frac{2}{3}, -\frac{1}{3}, 0, 1)$. Each column of \mathbf{g} corresponds to different ω and consecutive rows are node numbers. As mentioned before, $\lambda = 1$ is not taken into account in further calculations, so $\omega = \{\omega_1, \omega_2, \omega_3\} = \{\arccos(-\frac{2}{3}), \arccos(-\frac{1}{3}), \frac{\pi}{2}\}$. Now, having calculated \mathbf{g} and ω we are able to obtain $C(e, \omega)$ and $B(e, \omega)$ as described in Eq. (A3). To simplify the outcome we show it as matrices with rows denoted by graph edges and columns — by ω values:

$$\mathbf{C} = \begin{pmatrix} \omega_1 & \omega_2 & \omega_3 \\ e_{12} & -\frac{3\sqrt{26}}{26} & -\frac{3}{4} & \frac{\sqrt{2}}{2} \\ e_{13} & -\frac{1}{13}\sqrt{6}\sqrt{26} & -\frac{\sqrt{3}}{2} & 0 \\ e_{14} & -\frac{3\sqrt{26}}{26} & -\frac{3}{4} & \frac{\sqrt{2}}{2} \\ e_{23} & \frac{3\sqrt{26}}{26} & \frac{3}{4} & -\frac{\sqrt{2}}{2} \\ e_{24} & \frac{3\sqrt{26}}{26} & \frac{3}{4} & -\frac{\sqrt{2}}{2} \\ e_{34} & -\frac{1}{13}\sqrt{6}\sqrt{26} & \frac{\sqrt{3}}{2} & 0 \\ e_{32} & -\frac{3\sqrt{26}}{26} & \frac{3}{4} & \frac{\sqrt{2}}{2} \\ e_{31} & -\frac{3\sqrt{26}}{26} & \frac{3}{4} & \frac{\sqrt{2}}{2} \\ e_{41} & \frac{3\sqrt{26}}{26} & \frac{3}{4} & \frac{\sqrt{2}}{2} \\ e_{42} & \frac{3\sqrt{26}}{26} & \frac{3}{4} & \frac{\sqrt{2}}{2} \\ e_{43} & \frac{3\sqrt{26}}{26} & \frac{3}{4} & \frac{\sqrt{2}}{2} \end{pmatrix} \quad \mathbf{B} = \begin{pmatrix} \omega_1 & \omega_2 & \omega_3 \\ e_{12} & \arctan \frac{\sqrt{5}}{2} & -\arctan \frac{\sqrt{2}}{4} & \frac{\pi}{2} \\ e_{13} & -\arctan \sqrt{5} & \arctan \frac{\sqrt{2}}{2} & 0 \\ e_{14} & \arctan \frac{\sqrt{5}}{2} & -\arctan \frac{\sqrt{2}}{4} & -\frac{\pi}{2} \\ e_{23} & 0 & -\frac{\pi}{2} & 0 \\ e_{24} & 0 & \frac{\pi}{2} & 0 \\ e_{34} & -\arctan \sqrt{5} & \arctan \frac{\sqrt{2}}{2} & 0 \\ e_{32} & \arctan \frac{\sqrt{5}}{2} & -\arctan \frac{\sqrt{2}}{4} & \frac{\pi}{2} \\ e_{31} & \arctan \frac{\sqrt{5}}{2} & -\arctan \frac{\sqrt{2}}{4} & -\frac{\pi}{2} \\ e_{41} & 0 & -\frac{\pi}{2} & 0 \\ e_{42} & 0 & \frac{\pi}{2} & 0 \end{pmatrix} \quad (\text{A7})$$

Each column of matrix \mathbf{C} needs to be divided by a cor-

responding value of $\rho(\omega)$ given by Eq. (A4), i.e., in the

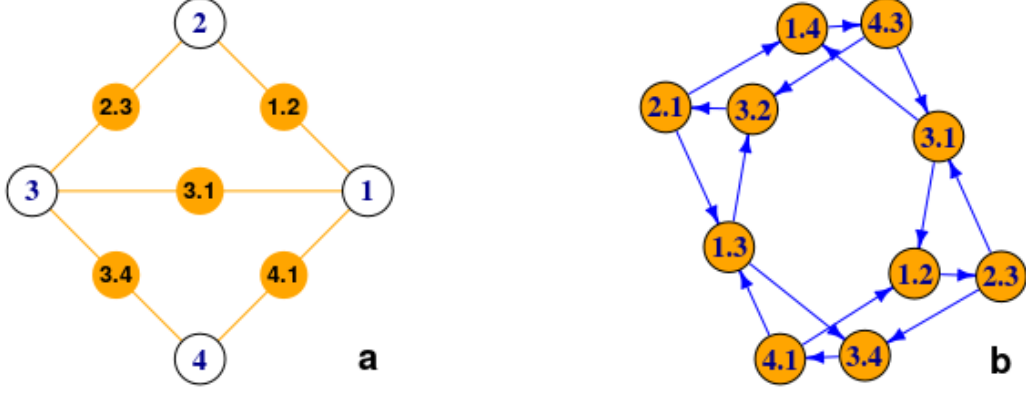


FIG. 10. (a) An example of a simple graph consisting of $|V| = 4$ nodes and $|E| = 5$ edges. (b) Oriented Line Graph obtained from the graph depicted in panel (a).

case of the exemplary graph $\rho = \{\frac{15}{13}, \frac{3}{2}, 1\}$. In this way we possess full information needed to evaluate values of u_1 .

Figure 10b presents an Oriented Line Graph obtained from the graph shown in Fig. 10a, its adjacency matrix \mathbf{A}_{olg} being simply

$$\mathbf{A}_{olg} = \begin{matrix} & \begin{matrix} e_{12} & e_{13} & e_{14} & e_{21} & e_{23} & e_{31} & e_{32} & e_{34} & e_{41} & e_{43} \end{matrix} \\ \begin{matrix} e_{12} \\ e_{13} \\ e_{14} \\ e_{21} \\ e_{23} \\ e_{31} \\ e_{32} \\ e_{34} \\ e_{41} \\ e_{43} \end{matrix} & \begin{pmatrix} 0 & 0 & 0 & 0 & 1 & 0 & 0 & 0 & 0 & 0 \\ 0 & 0 & 0 & 0 & 0 & 0 & 1 & 0 & 1 & 0 \\ 0 & 0 & 0 & 0 & 0 & 0 & 0 & 0 & 0 & 1 \\ 0 & 1 & 1 & 0 & 0 & 0 & 0 & 0 & 0 & 0 \\ 0 & 0 & 0 & 0 & 0 & 1 & 0 & 1 & 0 & 0 \\ 1 & 0 & 1 & 0 & 0 & 0 & 0 & 0 & 0 & 0 \\ 0 & 0 & 0 & 1 & 0 & 0 & 0 & 0 & 0 & 0 \\ 0 & 0 & 0 & 0 & 0 & 0 & 0 & 0 & 1 & 0 \\ 1 & 1 & 0 & 0 & 0 & 0 & 0 & 0 & 0 & 0 \\ 0 & 0 & 0 & 0 & 0 & 1 & 1 & 0 & 0 & 0 \end{pmatrix} \end{matrix} \quad (\text{A8})$$

We deliberately refrain from showing the full matrix $\tilde{\mathbf{D}}_{olg}$ of eigenvectors of \mathbf{A}_{olg} as in our case $|E| - |V| = 1$ so there is exactly one eigenvector corresponding to $\lambda = -1$ namely

$$\mathbf{C}_\pi = \begin{pmatrix} \frac{e_{12}}{4} & \frac{e_{13}}{4} & \frac{e_{14}}{4} & \frac{e_{21}}{4} & \frac{e_{23}}{4} & \frac{e_{31}}{4} & \frac{e_{32}}{4} & \frac{e_{34}}{4} & \frac{e_{41}}{4} & \frac{e_{43}}{4} \end{pmatrix} \quad (\text{A9})$$

It is now easy to check that if substitute Eq. (A2) with the calculated matrices \mathbf{C} , \mathbf{B} , ω and \mathbf{C}_π and assume that the wave is initially localised on edge $f = \{1, 2\}$ and $t = 0$, the amplitude $u = 1$ for $e = f = \{1, 2\}$ and $u = 0$ in any other case, as expected. The first 10 steps of propagation can be depicted in Fig. 11 (the wave moves toward $v = 2$).

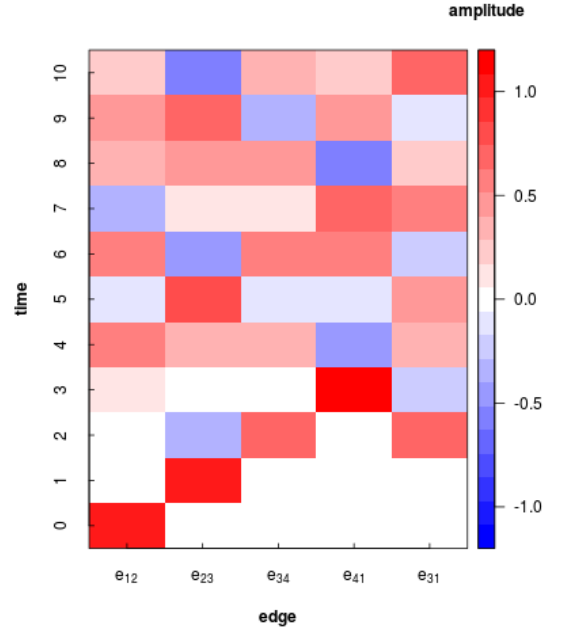


FIG. 11. Wave propagation on a graph shown in Fig. 10a for first 10 time steps (initial condition: a Gaussian wave fully contained on edge $f = \{1, 2\}$ moving toward vertex $v = 2$).

Appendix B: Principal component analysis

Principal components are a sequence of projections of the set of data in \mathbb{R}^p , mutually uncorrelated and ordered in variance in \mathbb{R}^q where $q \leq p$ [68]. In other words we transform the feature space such that it becomes orthogonal and each consecutive feature is aligned in the direction maximising the variance of the data and has more variance than the last. We do that by minimising

the reconstruction error, i.e. solving:

$$\min_{\mathbf{V}_q} \sum_{i=1}^N ||(x_i - \bar{x}) - \mathbf{V}_q \mathbf{V}_q^T (x_i - \bar{x})||^2 \quad (\text{B1})$$

where \mathbf{V}_q is a $p \times q$ matrix with q orthogonal unit vectors as columns. A $p \times p$ matrix $\mathbf{V}_q \mathbf{V}_q^T$ is the *transformation matrix* that maps each p -dimensional observation into its q -rank reconstruction. In our case specifically $p = q = 100$ and the examples of transformation matrices are represented as heat-maps in Fig. 3 and 4. In general PCA is known to be a quick and easy method to (i) perform dimensional reduction, (ii) help to visualise high-dimensional data and (iii) aggregate high-dimensional data into a possibly single measure (see, e.g., [69–71]).

Appendix C: K-nearest neighbours

In K-NN classification method the class estimation $\hat{y}(x)$ of a given sample x is taken as a majority vote amongst the member of $N_K(x)$ - the neighbourhood of x defined as K points closest to x [68, 72]. To determine which points are closest a metric must be chosen and for the purposes of this paper a Euclidean distance was used. In our case specifically each observation is a graph represented by its WPS, i.e. each graph is a point in a 100-dimensional space.

Appendix D: Fourier analysis

Fourier analysis allows us to convert a given time dependent signal $f(t)$ onto a frequency domain into $\hat{f}(\omega)$ via a Fourier transform and thus acquire the frequency distribution of said signal as it becomes a linear combination of trigonometric functions each corresponding to a particular frequency. A discrete Fourier transform is as name suggest a discrete version where integration is replaced by summation [73]. Therefore we consider a problem where one wants to express $f(t)$ as a complex Fourier series:

$$\hat{f}(\omega) = \sum_{k=0}^{N-1} f(k) e^{2\pi i \omega / N} \quad (\text{D1})$$

This procedure as it stands would require N^2 operations (where each operation is a complex multiplication followed by a complex addition), however, Cooley and Tukey in [57] presented a method known as the *fast Fourier transform* that allows to do it in less than $2N \log_2 N$.

Appendix E: Real world networks

We use three real world networks to test the Fourier transform approach.

Vickers et al. [54] collected data from 29 7th grade students from Victoria, Australia. Students were asked to nominate classmates in several categories, three of which were used to construct this 3-layer network. These three categories were determined by questions - Who do you get on with in the class? Who are your best friends in the class? Who would you prefer to work with? The graph has 29 nodes and 740 edges in total.

Krackhardt [58] took a record of relationship between managers in a high-tech company. The graph has 21 nodes and 312 edges in a 3-layer form. Each layer represents a relationship (advice, friendship, "reports to").

Chen et al. [59] presented a *Caenorhabditis elegans* multiplex connectome network with 3 layers, 279 nodes and 5863 edges. Each layer corresponds to a different synaptic junction: electric, chemical monadic, and polyadic.

Appendix F: Peak detection using a wavelet transform

A wavelet transform is an analogous procedure to the Fourier transform in the sense that we represent a given signal as an orthonormal series [74]. In case of Fourier those are sine and cosine while in the wavelet those are the eponymous wavelets. A wavelet is a particularly chosen function that is localised, i.e. it has a finite width the its family can compose an orthonormal basis for the signal - $s(t)$.

$$C(a, b) = \int_{\mathcal{R}} s(t) \frac{1}{\sqrt{a}} \psi\left(\frac{t-b}{a}\right) dt, \quad a \in \mathcal{R}^+, b \in \mathcal{R} \quad (\text{F1})$$

In our case the wavelet - ψ - was a Morlet (also known as the mexican hat) one as per the procedure described in [60] which (simplified) is as follows: perform a continuous wavelet transform (CWT) on the signal, identify the ridge lines by linking local maxima of CWT at each scale level, identify the peaks based on the ridge lines with three rules (quoted verbatim): "(1) The scale corresponding to the maximum amplitude on the ridge line, which is proportional to the width of the peak, should be within a certain range; (2) The SNR should be larger than a certain threshold; (3) The length of ridge lines should be larger than a certain threshold;". Here SNR is a *signal to noise ratio*.

- mulation of multilayer networks. *Physical Review X*, 3(4):041022, 2013.
- [2] Manlio De Domenico, Clara Granell, Mason A Porter, and Alex Arenas. The physics of spreading processes in multilayer networks. *Nature Physics*, 12(10):901–906, 2016.
 - [3] Guilherme Ferraz de Arruda, Francisco A Rodrigues, and Yamir Moreno. Fundamentals of spreading processes in single and multilayer complex networks. *Physics Reports*, 756:1–59, 2018.
 - [4] Mikko Kivelä, Alex Arenas, Marc Barthélemy, James P Gleeson, Yamir Moreno, and Mason A Porter. Multilayer networks. *Journal of complex networks*, 2(3):203–271, 2014.
 - [5] Stefano Boccaletti, Ginestra Bianconi, Regino Criado, Charo I Del Genio, Jesús Gómez-Gardenes, Miguel Romance, Irene Sendina-Nadal, Zhen Wang, and Massimiliano Zanin. The structure and dynamics of multilayer networks. *Physics Reports*, 544(1):1–122, 2014.
 - [6] Alain Barrat, Marc Barthélemy, and Alessandro Vespignani. *Dynamical processes on complex networks*. Cambridge university press, 2008.
 - [7] Romualdo Pastor-Satorras, Claudio Castellano, Piet Van Mieghem, and Alessandro Vespignani. Epidemic processes in complex networks. *Reviews of modern physics*, 87(3):925, 2015.
 - [8] Andrey Lokhov. Reconstructing parameters of spreading models from partial observations. In *Advances in Neural Information Processing Systems*, pages 3467–3475, 2016.
 - [9] Mateusz Wilinski and Andrey Y Lokhov. Scalable learning of independent cascade dynamics from partial observations. *arXiv preprint arXiv:2007.06557*, 2020.
 - [10] Jure Leskovec and Andreas Krause. Inferring networks of diffusion and influence. In *KDD10*, 2010.
 - [11] Jiin Woo, Jungseul Ok, and Yung Yi. Iterative learning of graph connectivity from partially-observed cascade samples. In *Proceedings of the Twenty-First International Symposium on Theory, Algorithmic Foundations, and Protocol Design for Mobile Networks and Mobile Computing*, pages 141–150, 2020.
 - [12] Jean Pouget-Abadie and Thibaut Horel. Inferring graphs from cascades: A sparse recovery framework. In *Proceedings of the 24th International Conference on World Wide Web*, pages 625–626, 2015.
 - [13] Bruno Abrahao, Flavio Chierichetti, Robert Kleinberg, and Alessandro Panconesi. Trace complexity of network inference. In *Proceedings of the 19th ACM SIGKDD international conference on Knowledge discovery and data mining*, pages 491–499, 2013.
 - [14] Vincent Gripon and Michael Rabbat. Reconstructing a graph from path traces. In *2013 IEEE International Symposium on Information Theory*, pages 2488–2492. IEEE, 2013.
 - [15] Manuel Gomez-Rodriguez, Jure Leskovec, and Andreas Krause. Inferring networks of diffusion and influence. *ACM Transactions on Knowledge Discovery from Data (TKDD)*, 5(4):1–37, 2012.
 - [16] Praneeth Netrapalli and Sujay Sanghavi. Learning the graph of epidemic cascades. *ACM SIGMETRICS Performance Evaluation Review*, 40(1):211–222, 2012.
 - [17] Alfredo Braunstein, Alessandro Ingrosso, and Anna Paola Muntoni. Network reconstruction from infection cascades. *Journal of the Royal Society Interface*, 16(151):20180844, 2019.
 - [18] LG Gajewski, Krzysztof Suchecki, and JA Hołyst. Multiple propagation paths enhance locating the source of diffusion in complex networks. *Physica A: Statistical Mechanics and its Applications*, 519:34–41, 2019.
 - [19] Robert Paluch, Xiaoyan Lu, Krzysztof Suchecki, Bolesław K Szymański, and Janusz A Hołyst. Fast and accurate detection of spread source in large complex networks. *Scientific reports*, 8(1):1–10, 2018.
 - [20] Robert Paluch, Łukasz G Gajewski, Janusz A Hołyst, and Bolesław K Szymański. Optimizing sensors placement in complex networks for localization of hidden signal source: A review. *Future Generation Computer Systems*, 112:1070–1092, 2020.
 - [21] Lucas Lacasa, Inés P. Mariño, Joaquin Miguez, Vincenzo Nicosia, Édgar Roldán, Ana Lisica, Stephan W. Grill, and Jesús Gómez-Gardeñes. Multiplex decomposition of non-markovian dynamics and the hidden layer reconstruction problem. *Physical Review X*, 8(3), Aug 2018.
 - [22] Peter Kuchment. Quantum graphs: I. Some basic structures. *Waves in Random media*, 14(1):S107–128, 2004. Publisher: Taylor & Francis.
 - [23] Peter Kuchment. Quantum graphs: II. Some spectral properties of quantum and combinatorial graphs. *Journal of Physics A: Mathematical and General*, 38(22):4887, 2005. Publisher: IOP Publishing.
 - [24] Peter Kuchment. Quantum graphs: an introduction and a brief survey. *arXiv preprint arXiv:0802.3442*, 2008.
 - [25] Gregory Berkolaiko and Peter Kuchment. *Introduction to quantum graphs*. American Mathematical Soc., 2013. Issue: 186.
 - [26] Joel Friedman and Jean-Pierre Tillich. Wave equations for graphs and the edge-based Laplacian. *Pacific Journal of Mathematics*, 216(2):229–266, 2004. Publisher: Mathematical Sciences Publishers.
 - [27] Norman E Hurt. *Mathematical physics of quantum wires and devices: From spectral resonances to Anderson localization*, volume 506. Springer Science & Business Media, 2013.
 - [28] Linus Pauling. The diamagnetic anisotropy of aromatic molecules. *The Journal of Chemical Physics*, 4(10):673–677, 1936.
 - [29] Peter Kuchment. Graph models for waves in thin structures. *Waves in random media*, 12(4):R1–R24, 2002.
 - [30] Jacob Biamonte, Mauro Faccin, and Manlio De Domenico. Complex networks from classical to quantum. *Communications Physics*, 2(1):1–10, 2019. Publisher: Nature Publishing Group.
 - [31] Pavel Exner and Olaf Post. Quantum networks modelled by graphs. In *AIP Conference Proceedings*, volume 998, pages 1–17. American Institute of Physics, 2008.
 - [32] Mauro Faccin, Piotr Migdał, Tomi H Johnson, Ville Bergholm, and Jacob D Biamonte. Community detection in quantum complex networks. *Physical Review X*, 4(4):041012, 2014. Publisher: APS.
 - [33] Mauro Faccin, Tomi Johnson, Jacob Biamonte, Sabre Kais, and Piotr Migdał. Degree distribution in quantum walks on complex networks. *Physical Review X*, 3(4):041007, 2013. Publisher: APS.
 - [34] Martí Cuquet and John Calsamiglia. Entanglement percolation in quantum complex networks. *Physical review letters*, 103(24):240503, 2009. Publisher: APS.
 - [35] Furqan Aziz, Richard C Wilson, and Edwin R Hancock. A wave packet signature for complex networks. *Journal*

- of *Complex Networks*, 7(3):346–374, June 2019.
- [36] Vadim Kostykin, Jürgen Pothoff, and Robert Schrader. Finite propagation speed for solutions of the wave equation on metric graphs. *Journal of Functional Analysis*, 263(5):1198–1223, 2012. Publisher: Elsevier.
 - [37] Sergio Gomez, Albert Diaz-Guilera, Jesus Gomez-Gardenes, Conrad J Perez-Vicente, Yamir Moreno, and Alex Arenas. Diffusion dynamics on multiplex networks. *Physical review letters*, 110(2):028701, 2013.
 - [38] Albert Sole-Ribalta, Manlio De Domenico, Nikos E Kouvaris, Albert Diaz-Guilera, Sergio Gomez, and Alex Arenas. Spectral properties of the laplacian of multiplex networks. *Physical Review E*, 88(3):032807, 2013.
 - [39] Furqan Aziz, Richard C Wilson, and Edwin R Hancock. Analysis of wave packet signature of a graph. In *International Conference on Computer Analysis of Images and Patterns*, pages 128–136. Springer, 2013.
 - [40] Furqan Aziz, Richard C Wilson, and Edwin R Hancock. Graph characterization using gaussian wave packet signature. In *International Workshop on Similarity-Based Pattern Recognition*, pages 176–189. Springer, 2013.
 - [41] Richard C. Wilson, Furqan Aziz, and Edwin R. Hancock. Eigenfunctions of the edge-based laplacian on a graph. *Linear Algebra and its Applications*, 438(11):4183 – 4189, 2013.
 - [42] Isaac Pesenson. Analysis of band-limited functions on quantum graphs. *Applied and Computational Harmonic Analysis*, 21(2):230–244, 2006. Publisher: Elsevier.
 - [43] Isaac Pesenson. Band limited functions on quantum graphs. *Proceedings of the American Mathematical Society*, 133(12):3647–3655, 2005.
 - [44] Pavel Exner and Diana Barseghyan. Spectral analysis of Schrödinger operators with unusual semiclassical behavior. *Acta Polytechnica*, 53(3), 2013.
 - [45] Carla Cattaneo. The spectrum of the continuous Laplacian on a graph. *Monatshefte für Mathematik*, 124(3):215–235, 1997. Publisher: Springer.
 - [46] Mark Kac. Can one hear the shape of a drum? *The american mathematical monthly*, 73(4P2):1–23, 1966.
 - [47] Carolyn Gordon, Peter Perry, and Dorothee Schueth. Isospectral and isoscattering manifolds: a survey of techniques and examples. *Contemporary Mathematics*, 387:157–180, 2005.
 - [48] Ram Band, Adam Sawicki, and Uzy Smilansky. Scattering from isospectral quantum graphs. *Journal of Physics A: Mathematical and Theoretical*, 43(41):415201, 2010.
 - [49] R Band, A Sawicki, and U Smilansky. Note on the role of symmetry in scattering from isospectral graphs and drums. *Acta Physica Polonica A*, 120(6A), 2011.
 - [50] Oleh Hul, Michał Ławniczak, Szymon Bauch, Adam Sawicki, Marek Kuś, and Leszek Sirko. Are scattering properties of graphs uniquely connected to their shapes? *Phys. Rev. Lett.*, 109:040402, Jul 2012.
 - [51] Uzy Smilansky. Delay-time distribution in the scattering of time-narrow wave packets.(i). *Journal of Physics A: Mathematical and Theoretical*, 50(21):215301, 2017.
 - [52] Uzy Smilansky and Holger Schanz. Delay-time distribution in the scattering of time-narrow wave packets (ii)—quantum graphs. *Journal of Physics A: Mathematical and Theoretical*, 51(7):075302, 2018.
 - [53] Michael Robinson. Inverse problems in geometric graphs using internal measurements, 2010.
 - [54] M Vickers and S Chan. Representing classroom social structure. *Victoria Institute of Secondary Education, Melbourne*, 1981.
 - [55] Joel Friedman and Jean-Pierre Tillich. Calculus on graphs. *arXiv preprint cs/0408028*, 2004.
 - [56] Ulrik Brandes. A faster algorithm for betweenness centrality. *Journal of mathematical sociology*, 25(2):163–177, 2001.
 - [57] James W Cooley and John W Tukey. An algorithm for the machine calculation of complex fourier series. *Mathematics of computation*, 19(90):297–301, 1965.
 - [58] David Krackhardt. Cognitive social structures. *Social networks*, 9(2):109–134, 1987.
 - [59] Beth L Chen, David H Hall, and Dmitri B Chklovskii. Wiring optimization can relate neuronal structure and function. *Proceedings of the National Academy of Sciences*, 103(12):4723–4728, 2006.
 - [60] Pan Du, Warren A. Kibbe, and Simon M. Lin. Improved peak detection in mass spectrum by incorporating continuous wavelet transform-based pattern matching. *Bioinformatics*, 22(17):2059–2065, 07 2006.
 - [61] Moody Chu, Moody T Chu, Gene Golub, and Gene H Golub. *Inverse eigenvalue problems: theory, algorithms, and applications*, volume 13. Oxford University Press, 2005.
 - [62] Gabriele Steidl and Maximilian Winkler. A new constrained optimization model for solving the nonsymmetric stochastic inverse eigenvalue problem. *arXiv preprint arXiv:2004.07330*, 2020.
 - [63] Filippo Cacace, Alfredo Germani, and Costanzo Manes. Karpelevich theorem and the positive realization of matrices. In *2019 IEEE 58th Conference on Decision and Control (CDC)*, pages 6074–6079. IEEE, 2019.
 - [64] Zhi Zhao, Xiao-Qing Jin, and Zheng-Jian Bai. A geometric nonlinear conjugate gradient method for stochastic inverse eigenvalue problems. *SIAM Journal on Numerical Analysis*, 54(4):2015–2035, 2016.
 - [65] Robert Orsi. Numerical methods for solving inverse eigenvalue problems for nonnegative matrices. *SIAM Journal on Matrix Analysis and Applications*, 28(1):190–212, 2006.
 - [66] Rubén J Sánchez-García, Emanuele Cozzo, and Yamir Moreno. Dimensionality reduction and spectral properties of multilayer networks. *Physical Review E*, 89(5):052815, 2014.
 - [67] Emanuele Cozzo, Guilherme Ferraz de Arruda, Francisco A Rodrigues, and Yamir Moreno. Multilayer networks: metrics and spectral properties. In *Interconnected Networks*, pages 17–35. Springer, 2016.
 - [68] Trevor Hastie, Robert Tibshirani, and Jerome Friedman. *The elements of statistical learning: data mining, inference, and prediction*. Springer Science & Business Media, 2009.
 - [69] ŁG Gajewski, J Chołowiecki, and JA Hołyst. Key courses of academic curriculum uncovered by data mining of students’ grades. *Acta Physica Polonica, A.*, 129(5), 2016.
 - [70] Julian Sienkiewicz, Krzysztof Soja, Janusz A Hołyst, and Peter MA Sloot. Categorical and geographical separation in science. *Scientific reports*, 8(1):1–12, 2018.
 - [71] Jan Chołowiecki, Julian Sienkiewicz, Naum Dretnik, Gregor Leban, Mike Thelwall, and Janusz A. Hołyst. A calibrated measure to compare fluctuations of different entities across timescales. *Scientific Reports*, 10(1):20673, November 2020.

- [72] K. N. Stevens, Prof M. Eden, I. Pollack, L. Ficks, Information Of Multidimensional, Auditory Displays, C. W. Ericson, Multidimensional Stimulus Differences, and P. E. Hart. Nearest neighbor pattern classification, 1953.
- [73] George B Arfken and Hans J Weber. Mathematical methods for physicists, 1999.
- [74] Ingrid Daubechies. *Ten lectures on wavelets*. SIAM, 1992.